Measurement report: Changes in light absorption and molecular composition of water-soluble humic-like substances during a winter haze bloom-decay process in Guangzhou, China

Chunlin Zou[1,3], Tao Cao[1,3], Meiju Li[1,3], Jianzhong Song[1,2,4,*], Bin Jiang[1,2], Wanglu Jia[1,2], Jun Li[1,2], Xiang Ding[1,2], Zhiqiang Yu[1,2,4], Gan Zhang[1,2], Ping'an Peng[1,2,3,4]

[1]State Key Laboratory of Organic Geochemistry and Guangdong Provincial Key Laboratory of Environmental Protection and Resources Utilization, Guangzhou Institute of Geochemistry, Chinese Academy of Sciences, Guangzhou 510640, China

[2]CAS Center for Excellence in Deep Earth Science, Guangzhou 510640, China

[3]University of Chinese Academy of Sciences, Beijing 100049, China

[4]Guangdong-Hong Kong-Macao Joint Laboratory for Environmental Pollution and Control, Guangzhou 510640, China

*_Correspondence to_: Jianzhong Song (songjzh@gig.ac.cn)

Abstract

Water-soluble humic-like substances (HULIS) absorb light in near-UV and visible wavelengths and exert significant influence on the atmospheric environment and climate. However, knowledge on HULIS evolution during haze bloom-decay process is limited. Herein, $PM_{2.5}$ samples were obtained during a winter haze event in Guangzhou, China, and light absorption and molecular composition of HULIS were investigated by UV-vis spectrophotometry and ultrahigh-resolution mass spectrometry. Compared with HULIS in clean days, the absorption coefficients (Abs_{365}) of HULIS in haze days were significantly higher but the mass absorption efficiencies (MAE_{365}) were relatively lower, suggesting diverse and dynamic absorption properties of HULIS during haze episodes. The CHO and CHON compounds were the most abundant components in HULIS, followed by CHOS, CHONS, and CHN. Haze HULIS presented comparatively higher molecular weight, lower aromaticity index (AI_{mod}), and higher O/C_w, O/N_w, and O/S_w ratios, indicating that HULIS fractions undergo relatively higher oxidation during haze days than clean days. Moreover, CHON and CHO compounds with high AI_{mod} were the major potential chromophores in HULIS and significantly contributed to HULIS light absorption. It's worth noting that the proportions of these chromophores were decreased during haze event, mainly owing to their higher oxidation during haze episode. Besides, accumulated contribution of organic compounds emitted from vehicles and formed from reactions of bio-VOCs also diluted light-absorbing compounds in haze HULIS. These findings help to understand HULIS evolution during haze bloom-decay process in the subtropic region of China.

1. Introduction

Water-soluble humic-like substances (HULIS), belonging to a class of highly complex organic compounds with physical/chemical properties similar to humic substances in natural aquatic/soil environments, which constitute 30%–70% of water-soluble organic compounds in ambient aerosols and are responsible for > 70% of light absorption (at 365 nm) in water-soluble brown carbon (BrC) (Graber and Rudich, 2006; Laskin et al., 2015; Huang et al., 2018). They are thought to be comprised of aromatic structures containing aliphatic side chains and oxygenated functional groups such as hydroxyl, carboxyl, nitrate, and organosulfate groups (Lin et al., 2012; Song et al., 2018; Zeng et al., 2020). HULIS are ubiquitously identified in atmospheric aerosols, fog, cloud, and rain water, and have been demonstrated to play significant effects on both atmospheric environment and climate (Bianco et al., 2018; Wu et al., 2018; Zeng et al., 2021). In addition, HULIS exert adverse health effects because they can enhance the oxidative potential of organic aerosols (Chen et al., 2019; Ma et al., 2019).

In recent years, severe particulate pollution (i.e., haze events) frequently occur in some developing country such as China, which has drawn extensive public and scientific concerns (Huang et al., 2014; An et al., 2019; Zhang et al., 2020). According to An et al. (2019), contributions of organic aerosols, including primary organic aerosols and secondary organic aerosols (SOA), are significant for severe haze events; in particular, the contribution of SOA in China is expected to continuously increase because of stronger chemical reactions in the atmosphere. HULIS are an important component in organic aerosols, which originate from a variety of primary emissions (e.g., biomass burning (BB), coal combustion, off-road engine emission) (Fan et al., 2016; Cui et al.,

2019; Tang et al., 2020) and secondary chemical oxidation of biogenic and anthropogenic volatile organic compounds (VOCs) (Yu et al., 2016; Tomaz et al., 2018) and soot (Fan et al., 2020). During the haze episode, a number of chemical processes occur in aqueous phase (Wong et al., 2017, 2019; Wu et al., 2018) and gas phase (Sumlin et al., 2017), which lead to significant changes in chemical composition and light absorption properties of HULIS. For instance, recent studies on oxidation of BB-derived BrC have indicated that although both enhancement and bleaching of BrC occur during aging, bleaching of BrC becomes dominant over a long period (Fan et al., 2020; Wong et al., 2017, 2019; Ni et al., 2021). However, multiphase reaction between carbonyl and amine has demonstrated rapid formation of light-absorbing organic compounds (Kampf et al., 2016). Nevertheless, it should be noted that these results were mainly obtained from laboratory experiments and may not reflect the complex evolution behavior of BrC in atmospheric environment.

High concentrations of HULIS have been determined during typical haze episodes in northern, eastern, and southern China (Fan et al., 2016; Win et al., 2020; Zhang et al., 2020; Wang et al., 2020), and have been demonstrated to significantly influence atmospheric visibility, environment, and photochemical process. Guangzhou is the biggest city in the Pearl River Delta (PRD), one of the most developed regions in China, and is located in the subtropical zone with a population of over 18 million people (Yu et al., 2017). Although a remarkable decline in atmospheric particulate matter ($PM_{2.5}$) pollution has been observed in recent years owing to strict regulatory controls, O_3 and VOCs still remain at higher levels and severe haze pollution caused by fine particulate matter frequently occur in winter (Huang et al., 2014; An et al., 2019; Li et al., 2019;

Yang et al., 2022). Several studies have investigated the optical, chemical, and molecular properties of HULIS in the PRD region (Lin et al., 2010, 2012; Fan et al., 2016; Liu et al., 2018; Jiang et al., 2020, 2021a,b). For example, the studies on the temporal variations of water-soluble HULIS in Guangzhou indicated that HULIS had higher concentrations and mass absorption efficiencies (MAE_{365}) in the winter, which were attributed to the increasing contribution of BB and secondary nitrate formation in the winter monsoon period (Fan et al., 2016; Jiang et al., 2020, 2021a). In addition, the molecular composition of HULIS (and BrC) in the PRD region were also investigated and demonstrated that the levels of unsaturated and aromatic structures are the important factor influencing their light absorption properties (Jiang et al., 2020, 2021b). However, detailed information regarding the evolution of light absorption and molecular composition of HULIS during haze events is still scarce.

Recently, ultrahigh-resolution Fourier transform ion cyclotron resonance mass spectrometry (FT-ICR MS) coupled with electrospray ionization (ESI) sources has been frequently employed to investigate the molecular characteristics of HULIS in ambient aerosols (Song et al., 2018, 2022; Tang et al., 2020; Zeng et al., 2021). Owing to its extremely high mass resolution and accuracy, this technique allows further exploration of the evolution of HULIS during haze event. The present study performed comprehensive characterization of HULIS in $PM_{2.5}$ collected during a haze event in Guangzhou, China. The abundances and light absorption properties of HULIS were first measured, and carbonaceous fractions, water-soluble ions, and levoglucosan (Lev) were determined. Subsequently, four HULIS samples collected during different haze stages were analyzed using FT-ICR MS operated in both ESI− and ESI+ modes. To the best of our knowledge,

the present study is the first to apply a combination of optical properties and molecular characterization by FT-ICR MS to investigate HULIS in a haze event in the subtropical zone of China. The results obtained provide novel insights into the evolution of HULIS during haze event, and are important for predicting the environmental and climatic effects of HULIS in South China.

2. Material and Methods

2.1. Aerosol sampling

The $PM_{2.5}$ samples were collected on the campus of Guangzhou Institute of Geochemistry, Chinese Academy of Sciences, Guangzhou, China (23.14N, 113.35E), which is an academic and residential region. Traffic emissions and residential activities are the potential pollution sources in the sampling area. The 24-h $PM_{2.5}$ sampling was conducted using a high-volume sampler (Tianhong Intelligent Instrument Plant, Wuhan, China, with a flow rate of 1.0 $m^3 min^{-1}$) during 7 to 30 January of 2018, and a total of 24 samples were collected on the prebaked quartz filters (20.3 × 25.4 cm^2, Whatman, Maidstone, UK). Field blank samples were collected by keeping a blank filter in the sampler without pumping air. Before sampling, the filters were wrapped in aluminum foil and prebaked at 450 ℃ for 6 h to remove carbonaceous impurities. Before and after sampling, the filters were weighed at 25 ℃ and 50% RH on a microbalance (Sartorius Model BP210D), with an accuracy of 0.01 mg. The $PM_{2.5}$ concentrations were determined by weighing the filters before and after collection. Finally, all filter samples were stored in a refrigerator at −20 ℃ until analysis. Meteorological data (http://www.wunderground.com/history/airport/ZGGG), including wind speed,

temperature, relative humidity, and concentrations of SO_2, O_3, and NO_2, for the sampling days are presented in Figure 1 and Table S1.

2.2. Isolation of HULIS

HULIS were isolated using a water extraction and solid-phase extraction (SPE) procedure as described previously (Zou et al., 2020). This method has been used in most previous studies because of its easy operation and high reliability and reproducibility and low limit of detection (Fan et al., 2002), therefore, it was also used in this study. Briefly, portions of the $PM_{2.5}$ samples (100 cm^2) were ultrasonically extracted with 50 mL of ultrapure water for 30 min. The extracts were filtered through a 0.22-μm PTFE syringe filter to remove the suspended insoluble particles. About 50 mL of water extracts were obtained from each sample, of which 20 mL was used for the isolation and analysis of HULIS, 20 mL for analysis of water-soluble organic carbon (WSOC), and the remainded extracts for the analysis of inorganic ions, respectively. Then, the 20 mL water extracts were adjusted to pH of 2 with HCl, and loaded on a preconditioned SPE cartridge (Oasis HLB, 200 mg/6 mL, Waters, USA). The hydrophilic fraction (i.e., inorganic ions, high-polar organic acids, etc) was removed with ultrapure water, whereas the relatively hydrophobic HULIS fraction was retained and eluted with 2% (v/v) ammonia/methanol. Finally, HULIS solution was evaporated to dryness with a gentle N_2 stream and redissolved with ultrapure water for the analysis.

It is noted that the HULIS here is the hydrophobic portion of water-soluble organic matter, which can be isolated with different types of SPE columns (e.g., HLB, C-18, DEAE, XAD-8, and PPL) (Fan et al., 2012, 2013; Lin et al., 2012; Zou et al., 2020; Jiang et al., 2020; Qin et al., 2022). Although each resin type has its special chemical properties,

the hydrophobic HULIS isolated with different sorbents were similar in chemical, molecular properties based on previous studies (Fan et al., 2012, 2013; Zou et al., 2020). Therefore, for better comparison with other studies, the hydrophobic fractions isolated by SPE methods were all termed as HULIS in the present paper.

2.3. Light absorption analysis

The absorption spectra of the WSOC and HULIS fractions were measured by a UV-vis spectrophotometer (UV-2600, Shimadzu) between 200 to 700 nm. Each spectrum was corrected for the filter blanks. The light absorption coefficients, absorption Ångström exponent (AAE) and mass absorption efficiency (MAE_{λ}) were calculated and the detailed methods are presented in the Supporting Information (SI).

2.4. Chemical analysis

For FT-ICR MS analysis, the HULIS samples were isolated from $PM_{2.5}$ collected during four periods: before haze days (clean-I days, 7–12 January), haze bloom days (haze-I days, 13–18 January), haze decay days (haze-II days, 19–24 January), and after haze days (clean-II days, 25–30 January). A filter punch (18 cm in diameter) was taken from every sample, and all the six samples in each period was combined for the isolation of HULIS fractions. The obtained HULIS samples were measured with an ESI FT-ICR MS (Bruker Daltonik GmbH, Bremen, Germany) equipped with a 9.4 T refrigerated actively shielded superconducting magnet. The system was operated in both ESI− and ESI+ modes. The scan range was set to m/z from 100 to 1000, with a typical mass-resolving power >450,000 at m/z 319 with <0.2 ppm absolute mass error. The mass spectra were calibrated externally with arginine clusters and internally recalibrated with

typical O_5-class species peaks in DataAnalysis 4.4 (Bruker Daltonics). Due to the inherent differences in the ionization mechanisms between ESI- and ESI+ modes, the data detected by the two ionization modes can provide complementary information on the molecular composition of atmospheric HULIS (Lin et al., 2012; Lin et al., 2018). The details of data analysis are provided in the SI.

The amounts of organic carbon (OC) and elemental carbon (EC) were determined by a OC/EC analyzer (Sunset Laboratory Inc., USA) (Mo et al., 2018). The concentrations of WSOC and HULIS were determined by a TOC analyzer (Shimadzu TOC_VCPH, Kyoto, Japan). The water-soluble inorganic species (NO_3^-, SO_4^{2-}, Cl^-, NH_4^+, K^+, Na^+, Ca^{2+}, Mg^{2+},) were measured with a Dionex ICS-900 ion chromatography system (Thermo Fisher Scientific, USA) as described previously (Huang et al., 2018). The concentrations of Lev were analyzed with a gas chromatography–MS after derivatization with BSTFA and pyridine at 70 ℃ for 3 h (Huang et al., 2018). Detailed information regarding these measurements is provided in the SI.

3. Results and Discussion

3.1. Abundance and chemical composition of $PM_{2.5}$

Figure 1 shows the meteorological conditions, $PM_{2.5}$ concentration, and concentrations of major chemical constituents, including carbon fractions and water-soluble inorganic ions in $PM_{2.5}$ samples obtained during a haze bloom-decay process. Based on the variation in $PM_{2.5}$ concentration, these samples were categorized into four groups: clean-I days (before haze, 14–24 μg m^{-3}), haze-I days (haze bloom, 45–114 μg m^{-3}), haze-II days (haze decay, 58–115 μg m^{-3}), and clean-II days (after haze, 9–35 μg

199 m^{-3}). As indicated in Table S1 and Figure 1, the $PM_{2.5}$ concentrations increased from 18
200 ± 3.3 μg m^{-3} in clean-I days to 82 ± 26 and 84 ± 22 μg m^{-3} in haze-I and haze-II days,
201 respectively, and then decreased to 21 ± 10 μg m^{-3} in clean-II days. This finding
202 obviously indicated that the average $PM_{2.5}$ concentrations during the examined haze
203 episode are higher than the second-grade national ambient air quality standard in China
204 (75 μg m^{-3}, 24 h), whereas those during clean days are lower than the first-grade national
205 ambient air quality standard in China (35 μg m^{-3}, 24 h). However, the average $PM_{2.5}$
206 concentrations during the haze event are lower than those in the cities in winter haze,
207 including Shenyang (108 μg m^{-3}) (Zhang et al., 2020), and Nanjing (123 ± 28.5 μg m^{-3})
208 (Li et al., 2020), Beijing (158 μg m^{-3}) and Xi'an (345 μg m^{-3}) (Zhang et al., 2018).

209 As shown in Table S1, the average concentrations of OC and EC were 2.2–15 and
210 0.36–2.7 μgC m^{-3} in the four stages, respectively, implying that the distinct changes in
211 OC and EC were higher during haze episodes than those in clear days. During the entire
212 study period, WSOC concentration ranged from 0.5 to 12.5 μgC m^{-3} (4.3 ± 1.2 μgC m^{-3}),
213 which contributed to 53%–57% of OC in $PM_{2.5}$. The HULIS concentration noted in the
214 present study ranged from 0.15 to 6.1 μgC m^{-3} (2.2 ± 1.9 μgC m^{-3}), which was
215 comparable to those observed in the PRD region, such as Hong Kong (2.38 ± 1.62 μgC
216 m^{-3}) (Ma et al., 2019) , Guangzhou (2.4 ± 1.6 μgC m^{-3}) (Fan et al., 2016), and Heshan
217 (2.08 ± 1.16 μgC m^{-3}) (Jiang et al., 2020), but lower than those in northern cities of
218 China, such as Xi'an (12.4 ± 6.5 μgC m^{-3}) (Huang et al., 2020), Beijing (3.79 ± 3.03
219 μgC m^{-3}) (Mo et al., 2018), and Lanzhou (4.7 μgC m^{-3}) (Tan et al., 2016). As shown in
220 Figure 1, HULIS also exhibited obvious variations during the entire sampling period. The
221 average HULIS concentration was 0.46 ± 0.22 μgC m^{-3} in clean-I days, which sharply

222 increased to 4.5 ± 1.2 μgC m^{-3} in haze-I days, then decreased to 3.1 ± 1.2 μgC m^{-3} in
223 haze-II days, and rapidly declined to 0.75 ± 0.52 μgC m^{-3} in clean-II days. This result
224 was consistent with the changing trend of WSOC, OC, and EC. In addition, the
225 HULIS/WSOC ratios were about 0.50 ± 0.13 in the $PM_{2.5}$ samples, which are in broad
226 agreement with other studies showing that HULIS is the major fraction of WSOC (Fan et
227 al., 2016; Ma et al., 2019; Jiang et al., 2020).

228 As illustrated in Figure 1, obvious variations in chemical compositions were also
229 observed in these $PM_{2.5}$ samples. Secondary inorganic aerosols (SIA) (i.e., SO_4^{2-}, NO_3^-,
230 and NH_4^+), OC, and EC exhibited a similar variation during the entire study period, and
231 their contents sharply increased from 10 January in clean-I days to 13–18 January in
232 haze-I days, then slowly decreased in haze-II days, and finally reached lower levels in
233 clean-II days. It must be noted that the increasing rate of EC was similar to that of SIA in
234 haze-I days, indicating that direct emissions and atmospheric reactions may play similar
235 roles in $PM_{2.5}$ increase during this haze bloom period. As indicated in Figure 1f, the
236 highest values of NO_3^-/SO_4^{2-} were observed in haze-I days, implying the important
237 influence of traffic exhausts in the haze bloom period (Mo et al., 2018). In addition, the
238 high NO_2 and O_3 concentrations and the stable meteorological condition with high
239 temperature also led to the outburst of fine particulate pollution in this period. During
240 haze-II days, the SIA and OM contents in $PM_{2.5}$ slowly decreased, whereas the
241 concentrations of Na^+, Cl^-, and unidentified materials in $PM_{2.5}$ increased (Figure 1e,h),
242 suggesting that local contribution weakened and regional contribution via sea salt became
243 more important (Jiang et al., 2021a). This phenomenon was also observed to be
244 consistent with the changes in the pollutant sources transported by air masses. As

indicated in Figure S1, the $PM_{2.5}$ samples in haze-II days included some contributors transported from coastal area of eastern Guangdong Province and Fujian Province, and the $PM_{2.5}$ are likely to be enriched with sea salt materials and mineral dusts.

3.2. Light absorption

The light absorption properties of WSOC and HULIS (Figure 1d, i, j and Table S2) exhibited obvious temporal variations during the sampling period. The AAE values of WSOC and HULIS ranged from 4.1 to 6.4 and 5.6 to 6.6, respectively. The AAE values for HULIS were obviously higher than those for WSOC in the same sample (Figure 1i), indicating that light absorption of HULIS is more wavelength-dependent than that of WSOC. This difference may be related with the light-absorbing organic species in the isolated HULIS fractions have strong wavelength dependence than those in the original WSOC. Moreover, the AAE values of HULIS did not present significant variation during the entire haze process.

Light absorption at 365 nm (Abs_{365}) for WSOC and HULIS were 2.5 ± 2.0 and 1.8 ± 1.6 M m^{-1}, respectively (Table S2). HULIS contributed to about 72% of light absorption coefficients by WSOC, implying that they enriched the major light-absorbing components in WSOC. As shown in Figure 1d, the Abs_{365} values for HULIS presented obvious temporal variations. The $Abs_{365,HULIS}$ value was 0.55 ± 0.06 M m^{-1} in clean-I days, which first increased to 3.4 ± 1.5 M m^{-1} in haze-I days and then slowly decreased to 2.6 ± 0.85 M m^{-1} in haze-II days, and finally rapidly declined to 0.64 ± 0.32 M m^{-1} in clean-II days. This result was similar to the variations in the mass concentration of HULIS. Furthermore, the Abs_{365} values for HULIS in Guangzhou were found to be higher than those observed in southeastern Tibetan Plateau (0.38–1.0 M m^{-1}) (Zhu et al.,

2018), but obviously lower than those in Xi'an (7.6–36 M m^{-1}) (Shen et al., 2017) and Beijing, (3.7–10.1 M m^{-1}) (Du et al., 2014).

In general, MAE_{365} value can be used to assess the light absorption capacity of target organic compounds (Li et al., 2019). As shown in Figure 1j and Table S2, the average MAE_{365} value for WSOC was 1.0 ± 0.21 m^2 gC^{-1} (0.68–1.3 m^2 gC^{-1}), nearly same to 1.1 ± 0.27 m^2 gC^{-1} (0.77–1.8 m^2 gC^{-1}) for HULIS, during the entire sampling period. Moreover, the MAE_{365} values for HULIS measured in the present study were noted to be dropped in the ranges of those determined in Beijing (1.43 ± 0.33 m^2 g C^{-1}) (Mo et al., 2018), Xi'an (0.91–1.85m^2 g C^{-1}) (Yuan et al., 2021), and Hong Kong (1.84 ± 0.77 m^2 gC^{-1}) (Ma et al., 2019). The average MAE_{365} values for HULIS exhibited some temporal variations. The MAE_{365} values for HULIS were 0.91±0.03 and 0.95 ± 0.11 m^2 gC^{-1} in haze-I and haze-II days, respectively, which were lower than those (1.3 ± 0.22 and 1.3 ± 0.27 m^2 gC^{-1}, respectively) observed in clean-I and clean-II days, suggesting that HULIS have a relatively weaker light absorption capability in haze days. This finding is consistent with the results reported by Zhang et al. (2017), who found that the MAE_{365} values in the heating or non-heating seasons during hazy days were lower than those in clean days. These differences in MAE_{365} values may potentially contribute to the enhanced oxidation reaction that was derived by the increased O_3 levels and high temperature and relative humidity (RH) during haze days (Figure 1). This oxidation process would lead the chromophores containing C=C unsaturated bond to be severely degraded (Wang et al., 2017a; Zhang et al., 2017). Besides, an increase in additional sources for HULIS in the study area, such as weaker or non-light-absorbing compounds

formed by atmospheric oxidation, could also result in weaker light absorption of HULIS during the haze episode (Liu et al., 2018).

3.3. Molecular evolution of HULIS during the haze process

For an in-depth understanding of the variation in HULIS at molecular level during the haze process, the four HULIS samples collected in different stages of the haze process were analyzed by ESI FT-ICR MS in both negative and positive modes. As shown in Figure 2, thousands of peaks were detected in the mass range between m/z 100 and m/z 700, with the high intensity ions noted within m/z 150–400. It is obvious that some organic compounds with stronger arbitrary abundance were labeled, and their formulas, double bond equivalent (DBE), modified aromaticity index (AI_{mod}), and potential sources were listed in Table S3. Compounds a ($C_7H_7NO_3$) and b ($C_8H_6O_4$), both have high DBE values, which might be assigned to aromatics such as methylnitrophenol and phthalic acid, whereas compound d ($C_8H_{18}O_4S$) with low DBE value and high O/S ratio was probably aliphatic organosulfate. According to previous studies, these organic molecules might be derived from BB and diesel fuel and thereby these results suggested that both BB and vehicular emissions are important sources of BrC in ambient aerosols (Mohr et al., 2013; Riva et al., 2015; Blair et al., 2017). Furthermore, compound e ($C_{10}H_{17}NO_7S$) and compound f ($C_{10}H_{18}N_2O_{11}S$) in Table S3 were found to be identical to the oxidation products of monoterpenes, suggest that biogenic sources could contribute to the formation of HULIS (Surratt et al., 2008; Wang et al., 2019). Thus, HULIS could be affected by multiple sources during the haze process, possibly including BB, biogenic sources, and anthropogenic emissions.

312 The identified formulas could be divided into seven compound categories, namely,
313 CHO−, CHON−, CHOS−, and CHONS− detected in ESI− mode and CHO+, CHN+, and
314 CHON+ detected in ESI+ mode. As illustrated in Figure 2, the CHO compounds were the
315 most abundant group in all the HULIS, accounting for 43%–50% and 51%–57% of the
316 overall compounds detected in the ESI− and ESI+ modes, respectively. It must be noted
317 that relatively lower contents of CHO− were detected during the haze episode (haze-I and
318 haze-II days) and CHO+ molecules in haze-I HULIS. The CHON compounds were the
319 second most abundant group in all the HULIS. As shown in Figure 2, the relative content
320 of CHON− was 23% in clean-I days, which slightly increased to 24%–25% in haze
321 episode, and then decreased to 23% in clean-II days. In contrast, the relative content of
322 CHON+ compounds was 41% in clean-I days, which increased to 45% in haze-I days,
323 then fell to 42% in haze-II days and 41% in clean-II days. Both CHOS− and CHONS−
324 compounds were identified in all the four HULIS, accounting for 19%–22% and 8%–11%
325 of the total identified compounds, respectively. The CHN+ compounds were the least
326 abundant (1.3%–3.6%) in the four HULIS samples, and were relatively higher during the
327 haze episode, especially in haze-I days.

328 Tables S4 and S5 show the relative abundance weighted elemental ratios, molecular
329 weight (MW), DBE, AI_{mod}, and carbon oxidation state (OS_C) for the identified
330 compounds in HULIS. The MW_w values for HULIS determined in the ESI− mode in
331 haze-I and haze-II days were 302 and 283, respectively, which were higher than those in
332 clean-I and clean-II days (266 and 264, respectively). Similar variation was also observed
333 for MW_w for HULIS detected in ESI+ mode (Table S5). These results clearly indicated
334 that more higher MW compounds constituted HULIS obtained during the haze episode. It

has been reported that the low MW compounds (provided by size exclusion chromatography) are more susceptible to atmospheric oxidation processes, while the high MW compounds have relatively higher chemical resistance for BB aerosols (Di Lorenzo, et al., 2017; Wong et al., 2017; Dasari et al., 2019). Although the HULIS samples in this study were more complex than those in BB aerosols, it is expected that the high MW molecules mostly were the recalcitrant fraction in HULIS. Therefore, the HULIS compounds undergo higher oxidation during haze episode, and are thereby characterized by relatively high MW values.

Furthermore, the molecular properties of HULIS in different stages of haze process also exhibited some observable differences. As shown in Table S4, the HULIS samples in haze episode detected by ESI− mode presented relatively lower $AI_{mod,w}$ values and relatively higher O/C_w, O/N_w, and O/S_w ratios than those in clean days, indicating that haze HULIS exhibited relatively lower aromaticity and higher oxidation degree than clean HULIS. These differences can be attributed to the enhanced oxidation degradation of aromatic compounds (e.g., phenols, nitroaromatic compounds and polycyclic aromatic hydrocarbons (PAHs)) during the haze process. In addition, increased contribution from traffic emission and secondary reactions of bio-VOCs also decreased the aromaticity and increased the oxidation degree of HULIS (Liu et al., 2016; Tang et al., 2020). These changes in HULIS compounds led to the decrease in their MAE_{365} values during the haze episode, as described above (Zhong and Jang, 2014; Song et al., 2019).

3.3.1. CHO Compounds

The CHO compounds bear O-containing functional groups, and have been frequently detected in ambient aerosols. As shown in Figure 2, the CHO compounds were

the predominant component in the four HULIS samples, and the MW_w values for CHO− and CHO+ compounds were 247–288 and 236–272, respectively, with relatively higher MW_w values observed for the CHO group (CHO− and CHO+) in haze HULIS, especially in haze-I samples. This finding may be related to the stronger oxidation of HULIS during haze days, because the aqueous oxidation of biomass burning aerosols was found to yield high MW of organic products (Tomaz et al., 2018; Yu et al., 2016).

The OS_C is often used to describe the degree of oxidation of organic species in the atmosphere (Kroll et al., 2011; Tong et al., 2019). Figure 3 shows plots of OS_C versus carbon number for the CHO compounds. As indicated in the figure, CHO compounds exhibited OS_C from −2 to +1 with up to 40 carbon atoms. Kroll et al. (2011) proposed that compounds with OS_C between −0.5 and +1 and < 18 carbon atoms can be attributed to semi-volatile and low-volatile oxidized organic aerosols (SV-OOA and LV-OOA), which are mainly formed by complex oxidation reactions in atmosphere. Compounds with OS_C between −0.5 and −1.5 and 6–23 carbon atoms are related to primary biomass burning organic aerosol (BBOA). In addition, compounds with OS_C between −1 and −2 and ≥18 carbon atoms have been suggested to be hydrocarbon-like organic aerosols (HOA), which are regarded as primary combustion surrogate (Zhang et al., 2005; Kroll et al., 2011; Wang et al., 2017b).

As illustrated in Figure 3 and Table S6, most of the CHO− compounds clustered in the BBOA region, accounting for 40%–46% of the total CHO− compounds, thus suggesting that BB may be a major contributor to CHO compounds in HULIS. Figure 3 clearly indicates that the majority of aromatic and condensed aromatic compounds produced signals in the OS_C region between −0.5 and 1.0 and carbon number of 3–18

(Figure 3), which corresponded to SV-OOA and LV-OOA. The proportions of SV-OOA and LV-OOA accounted for 23%–28% and 1.9%–2.4% of the total CHO− compounds, respectively, and presented no significant variation. In contrast, the HOA components in haze-I days showed the highest abundance (18%), which were much higher than those (3.5%–4.5%) in haze-II, clean-I, and clean-II days. This finding indicated that the increase in the primary source is associated with fossil fuel combustion such as vehicle emissions during the haze bloom period (Zhang et al., 2005).

As shown in Figure 3, CHO+ compounds presented lower OS_C (from −2.0 to 1.0) than CHO− compounds. Most of the CHO+ compounds occurred in the BBOA region in all four HULIS samples, making up to 60%–72% of the total CHO+ compounds, which again suggesting that BB is an important contributor to CHO compounds in HULIS. The HOA among CHO+ compounds showed the same changing trends as those among CHO− compounds, and higher HOA abundance was observed during haze-I days. In addition, some high AI_{mod} values of aromatics were found in the regions A1+ and A2+ (Figure 3), which implied that the highest AI_{mod} values ($AI \geq 0.67$) with $DBE \geq 22$ were only detected during the haze days possibly owing to soot-derived materials or oxidized PAHs (Decesari et al., 2002; Kuang and Shang, 2020). It must be noted that the sampling site in the present study is influenced by traffic sources, the enhanced oxidation of vehicle-exhausted soot also results in the accumulation of water-soluble high aromatic organic species (Decesari et al., 2002).

3.3.2. CHON Compounds

In the present study, 1379–2217 and 2008–2943 formulas were assigned to CHON compounds identified in the ESI− and ESI+ spectra, respectively, which accounted for

404 23%–25% (ESI−) and 41%–45% (ESI+) of total identified compounds, respectively.
405 Relatively higher contents of CHON− compounds were obviously detected in HULIS
406 samples obtained during haze-I days, suggesting the occurrence of more N-containing
407 components in HULIS during haze bloom days. As shown in Tables S4 and S5, the
408 average MW_w values for CHON− and CHON+ compounds were 328 and 317 in haze-I
409 days, respectively, which were slightly higher than those determined in haze-II days and
410 all higher than those observed in clean-I and clean-II days. Meanwhile, the $AI_{mod,w}$ values
411 for CHON− in haze days were 0.31–0.34, which were slightly lower than those in clean
412 days (0.37 and 0.40). These findings indicated that more high MW CHON compounds
413 with lower aromatic structures were formed during the haze episode.

414 The O/N_w ratios for CHON− and CHON+ during haze-I and haze-II days were 5.3–
415 5.7 and 3.8, respectively, which were higher than those determined during the two clean
416 periods, confirming that these compounds were highly oxidized during the haze episode
417 (Tables S4 and S5). In general, compounds with $O/N \geq 3$ may indicate oxidized N groups
418 such as nitro ($–NO_2$) or nitrooxy ($–ONO_2$), whereas compounds with $O/N < 3$ may denote
419 the reduced N compounds (i.e., amines) (Lin et al., 2012; Song et al., 2018). In the
420 present study, most of the CHON compounds (79%–91% of CHON– compounds and
421 61%–64% of CHON+ compounds) exhibited $O/N \geq 3$, suggesting that high
422 concentrations of nitro compounds or organonitrates were contained in the CHON
423 compounds. Moreover, these compounds were more abundant in the CHON– group
424 during the haze episode (87%–91%), when compared with those during clean-I and
425 clean-II days (79%–82%), again implying that CHON– compounds undergo relatively
426 higher oxidization during the haze episode. As indicated in Figure 1, the increase in NO_2

was consistent with increased production of highly oxidized N-containing organic compounds (NOCs) during the haze episode, which suggested the significant contribution of NO_3-related multigenerational chemistry to organonitrate aerosol formation (Berkemeier et al., 2016).

The majority of aromatics and condensed aromatics produced clear signals in regions associated with SV-OOA and LV-OOA (Figure 4). BBOA also constituted a significant proportion (33%–39%) in the CHON– group, and a relatively lower BBOA content was observed in haze-I days. The abundance of HOA was relatively lower, accounting for 2.3%–7.8% of the total CHON compounds, and the relative abundance of HOA in haze-I days was much higher than that in haze-II, clean-I, and clean-II days, suggesting the accumulation of primary fossil fuel combustion during haze-I days.

The CHON+ compounds mainly occurred at the range of $-2.0 < OS_C < 1.5$, with average OS_C values of around −1.0 for each sample, clearly indicating that CHON+ compounds were relatively lower than CHON– compounds. Most of the CHON+ compounds were detected in the BBOA region, accounting for 60%−76% of the total $CHON^+$ compounds. The relative contribution of BBOA in haze-I days was lower than that in haze-II and clean days. Moreover, a large number of aromatic species were observed at the region B1+ (Figure 4), demonstrating that higher aromatic compounds were only detected in haze-I days, which may be related to soot or BC. Similar trend was also exhibited by CHO+ compounds, indicating the contribution of local combustion sources (e.g., traffic emission) during haze-I days.

3.3.3. CHOS and CHONS Compounds

In this study, 478–696 CHOS compounds and 306–589 CHONS compounds were identified in ESI– mode (Table S4). Among these S-containing compounds, >86% of the CHOS compounds had O/S ratios >4, whereas > 89% of the CHONS compounds presented O/S ratios >7, suggesting that these S-containing compounds were possibly organosulfates and nitrooxyorganosulfates. As listed in Table S4, the $AI_{mod,w}$ values for CHOS and CHONS were about 0.02 and 0.01 in the HULIS fraction, which were much lower than those for CHO and CHON. Almost 99% of the CHOS and CHONS compounds in the HULIS fraction had AI_{mod} values <0.5, while >93% of the CHONS compounds had AI_{mod} = 0, indicating that they were mainly comprised of aliphatic and olefinic organosulfates. These results are consistent with the previous findings that the major S-containing compounds among organic aerosols in Guangzhou are organosulfates formed by secondary oxidation reaction of long-chain alkenes/fatty acids with SO_2 (Jiang et al., 2020), which generally possessed long aliphatic carbon chains and a higher degree of oxidation. However, these compounds are different from the S-containing compounds detected during the hazy days in Beijing (Jiang et al., 2016; Mo et al., 2016), which were determined to be aliphatic organosulfates with low degree of oxidation and higher amounts of aromatics and PAH-derived organosulfates, having a strong correlation with anthropogenic emissions.

As described earlier, CHOS− and CHONS− compounds might be related to organosulfates or nitrooxyorganosulfates, which have been observed to be derived from atmospheric reactions of bio-VOCs such as α-pinene, limonene, and isoprene (Huang et al., 2018; Surratt *et al.*, 2008) and fossil fuel combustion including coal combustion, off-road engine emissions (Song et al., 2018, 2019; Cui et al., 2019). In the present study, the

relative contents of S-containing compounds (CHOS+CHONS) in the HULIS fraction in haze days were all higher than those in clean days (Figure 2). Moreover, the CHOS and CHONS compounds in haze HULIS always have relatively high relatively O/S ratios than those in clean HULIS. These findings suggested the relatively higher contribution of SO_2-related chemical oxidation during the haze event.

3.3.4. CHN Compounds

The N-bases (CHN) are usually identified in ambient aerosols and smokes from BB. In the present study, 110–165 CHN+ compounds were identified in ESI+ mode, with most of them (>86%) presenting DBE ≥ 2, suggesting that they might be nitrile and amine species (Lin et al., 2012). As shown in Figure 2, the abundances of CHN+ compounds were 2.0%–3.6% in the haze days, which were much higher than those noted in clean days (1.3%–1.4%), indicating higher contribution of CHN+ compounds to the HULIS fraction during the haze episode. The MW_w values for CHN+ compounds were 204–223, which were lower than those for the other groups (i.e., CHO+, CHON+) (Table S5). However, the average AI_{mod} values for N-bases (0.37–0.48) detected in the ESI+ mode were much higher than those for CHO+ (0.11–0.12) and CHON+ (0.20–0.22) compounds, implying that these reduced CHN+ compounds exhibited more unsaturated or aromatic structures.

To further understand the molecular distribution of CHN+ compounds during the haze process, van Krevelen (VK) diagrams were constructed by plotting the H/C ratio versus N/C ratio (Figure S2). It was obvious that this plot could separate the compound classes with different degree of AI. As shown in Figure S2, compounds (denoted in black color) in the upper region of the VK diagram had one N atom with DBE = 0, indicating

that they are aliphatic amines. It can be noted from Table S7 that the aliphatic group presented the lowest abundance in all the samples, suggesting that the CHN+ compounds possessed comparatively lower aliphatic structures. Olefinic compounds showed the highest abundance in the four samples, which accounted for 37%–51% of the total CHN+ compounds. Importantly, a large proportion of the compounds (>39%) exhibited high degree of AI (AI > 0.5) (Figure S2 and Table S7), suggesting a large amounts of aromatic structure and N-heterocyclic ring in HULIS. Moreover, the CHN+ compounds in haze-I days presented obviously lower content of aromatic structures than those in haze-II, clean-I, and clean-II days, signifying the relatively high contribution of fossil fuel combustion (which generally emits more low-aromatic CHN compounds) during the haze bloom episode(Song et al., 2022). In addition, the CHN+ group also constituted a large proportion of BBOA (Table S6), which indicated the significant contribution of BB. However, it must be noted that a relatively lower content of BBOA was detected during haze-I days, which was consistent with the changing trends of CHON- or CHON+ compounds during the haze episode. These results suggested the relatively lower contribution of BB during haze-I days, because quiet and stable weather conditions can prevent regional transport of BB sources during this stage (Wu et al., 2018).

3.4. Factors influencing light absorption and molecular characteristics of HULIS during the haze bloom-decay process

As described earlier, the light absorption properties of HULIS exhibited obvious variation during the haze bloom-decay process. The average Abs_{365} value for HULIS was 0.55 ± 0.06 M m^{-1} in clean-I days, which first increased to 3.4 ± 1.5 M m^{-1} in haze-I days, then slowly decreased to 2.6 ± 0.85 M m^{-1} in haze-II days, and finally rapidly declined to

518 0.64 ± 0.32 M m^{-1} in clean-II days. In general, the light absorption of HULIS can be
519 related to their chemical and molecular properties that are influenced by factors such as
520 sources, secondary formation, and aging process. The results of principal component
521 analysis (PCA) obviously showed a positive loading for principal component 1 (PC1),
522 and the Abs_{365} values for HULIS were clustered with EC, K_{bb}^{+}, Lev, NH_4^{+}, and NO_3^{-}
523 (Figure 5). These results suggested that BB and other sources such as new particle
524 formation could contribute to light absorption of HULIS (Huang et al., 2014; An et al.,
525 2019; Song et al., 2019). Similarly, the findings of Pearson correlation coefficient
526 analysis revealed that the Abs_{365} values for HULIS exhibited significant positive
527 correlations with K_{bb}^{+} ($r = 0.728$, $p < 0.01$) and Lev ($r = 0.800$, $p < 0.01$) (Table S8). As
528 Lev and K_{bb}^{+} are generally considered as tracers derived from BB, these results suggested
529 the significant contribution of BB to light absorption of HULIS. This observation was
530 also supported by the abundance of BBOA compounds detected in all the four HULIS
531 samples (Table S6). The significant positive relationships between the Abs_{365} values for
532 HULIS and secondary ions (i.e., NO_3^{-} ($r = 0.702$, $p < 0.01$), SO_4^{2-} ($r = 0.554$, $p < 0.05$),
533 and NH_4^{+} ($r = 0.899$, $p < 0.01$)) indicated the important impact of secondary formation on
534 the light absorption of HULIS. Besides, the Abs_{365} values for HULIS were also strongly
535 correlated with NO_2, O_3, and NO_2, which confirmed the important impact of atmospheric
536 oxidation reactions on the light absorption of HULIS.

537 It must be noted that MAE_{365} is a key parameter signifying the light absorption
538 ability of HULIS. As listed in Table S2, the MAE_{365} values for HULIS varied in different
539 stages, and were lower in haze days owing to the variation in the chemical and molecular
540 composition of HULIS during the haze bloom-decay process. Furthermore, the AI_{mod}

values for HULIS varied in different stages (Tables S4), and were relatively lower in haze days, indicating that haze HULIS have comparatively lower degree of conjugation or aromaticity. This finding suggested that the HULIS compounds may undergo higher oxidation during the haze episode, causing a decline in chromophores and reduction in the light absorption capacity of HULIS (Lin et al., 2017). Besides, the accumulated contribution of organic compounds from vehicle emission and secondary chemical reactions of bio-VOCs may also dilute light-absorbing compounds in haze HULIS (Tang et al., 2020; Liu et al., 2016).

Lin et al. (2018) reported that potential light-absorbing chromophores can be determined in the region between DBE = 0.5 × C (linear conjugated polyenes $C_xH_yC_2$) and DBE = 0.9 × C (fullerene-like hydrocarbons). In the present study, most of the high-intensity CHON, CHO, and CHN compounds with high AI values were clustered in potential BrC chromophore region (Figures S3 and S4), which mainly comprised CHON (46%–50% in ESI- mode and 56%–62% in ESI+ mode, respectively) and CHO (44%–48% in ESI- mode and 29%–38% in ESI+ mode, respectively) compounds (Table 1). Although the contribution of CHN+ compounds to BrC was relatively lower, the content of potential chromophores among the total CHN+ compounds was higher than those in CHON+ and CHO+ compounds. Therefore, these three groups of light-absorbing compounds (i.e., CHON+, CHN+, and CHO+ compounds) were further examined. As shown in Table 1, the Int_C/Int_{BrC} values of CHO− (i.e., content of CHO− chromophores in the total chromophores) decreased from 48% to 44% whereas the Int_C/Int_{BrC} values of CHON− increased from 46% to 50% during the haze bloom process. These findings indicated that more NOCs chromophores were formed during this stage in which higher

564 NO_2 concentration may be preferred for the formation of N-containing chromophores
565 such as nitrophenols. However, it must be noted that the proportions of both CHO− and
566 CHON− chromophores among the total identified compounds decreased from clean-I to
567 haze-I days, suggesting the occurrence of stronger photo-bleaching process during the
568 haze bloom stage (Zeng et al., 2020). Likewise, both CHO+ and CHON+ compounds
569 presented similar variation during the entire study period. In addition, the CHN+
570 compounds also exhibited higher Int_C/Int_{BrC} values during the haze bloom process and
571 suggesting the accumulated contribution from local combustion process. Furthermore, the
572 proportion of CHON+ chromophores in the total CHON+ compounds increased with the
573 decreasing content of CHN+ chromophores, may implying that some aromatic CHN
574 compounds were transformed to CHON+ compounds during the aging process.
575
576 **4. Conclusions**
577 This study investigated the evolution of light absorption and molecular properties of
578 HULIS during a winter haze bloom-decay process, and examined the key factors
579 affecting the light absorption of HULIS in Guangzhou, China. The results showed that
580 HULIS exhibited significant variation in light absorption during the haze bloom-decay
581 process. First, higher Abs_{365} values were observed in haze days, indicating the presence
582 of significant amounts of light-absorbing organic compounds during the haze episode.
583 However, the MAE_{365} values for HULIS in haze days were relatively lower than those in
584 clean days, suggesting the light absorption capabilities of HULIS were weakened during
585 the haze event. Furthermore, CHON and CHO compounds, exhibiting relatively higher
586 degree of conjugated structure, were the most abundant groups in all the HULIS samples,

and were also the major contributors to light absorption capacity of HULIS. Importantly, the molecular properties of HULIS dynamically varied during the entire haze episode. When compared with HULIS in clean days, those in haze days presented relatively lower AI_{mod} values and higher O/C_w, O/N_w, and O/S_w ratios, suggesting the predominance of compounds with low aromaticity and higher oxidation in HULIS during haze episode. These results indicated that HULIS compounds undergo relatively stronger oxidation during the haze days. Moreover, PCA and Pearson correlation analysis revealed that BB and secondary chemical formation both contributed to the variation in the light absorption properties of HULIS. Both primary sources (such as accumulated contribution of organic compounds formed from local traffic emission) and secondary sources (such as stronger chemical reactions) led to the rapid increase in HULIS during the haze bloom days. However, stronger oxidation of HULIS compounds were observed during the haze episode, and some potential BrC chromophores were degraded. In addition, the chemical reactions of bio-VOCs such as isoprene also diluted the light-absorbing compounds in HULIS.

Thus, the present study provides novel insights into the light and molecular evolution of HULIS during haze event, which are important for predicting the environmental and climatic effects of HULIS. However, as this study examined only one haze bloom-decay process in winter in Guangzhou, the results obtained may be not adequate for understanding all the haze episodes in South China. Therefore, there is a need for a comprehensive investigation of haze episode in different seasons and regions in future.

Data availability

The research data are available in the Harvard Dataverse (https://doi.org/10.7910/DVN/DYGYQT, Song, 2022).

Author contributions. J. Song and P. Peng designed the research together. C, Zou, T. Cao, and M. Li carried out the $PM_{2.5}$ sampling experiments. C, Zou and T. Cao extracted and analyzed the WSOC and HULIS samples. B. Jiang analyzed the HULIS samples by FT-ICR MS. C. Zou and J. Song wrote the paper. J. Li, X. Ding, Z Yu, and G. Zhang commented and revised the paper.

Competing interests. The authors declare that they have no conflict of interest

Acknowledgments. This study was supported by the National Natural Science Foundation of China (42192514 and 41977188), Guangdong Foundation for Program of Science and Technology Research (2020B1212060053), and Guangdong Foundation for Program of Science and Technology Research (2019B121205006).

References

An, Z., Huang, R. J., Zhang, R., Tie, X., Li, G., Cao, J., Zhou, W., Shi, Z., Han, Y., Gu, Z., and Ji, Y.: Severe haze in northern China: A synergy of anthropogenic emissions and atmospheric processes, Proc Natl Acad Sci USA, 116, 8657-8666, 10.1073/pnas.1900125116, 2019.

Berkemeier, T., Ammann, M., Mentel, T. F., Poschl, U., and Shiraiwa, M.: Organic nitrate contribution to new particle formation and growth in secondary organic aerosols from alpha-pinene ozonolysis, Environ Sci Technol, 50, 6334-6342, 10.1021/acs.est.6b00961, 2016.

Bianco, A., Deguillaume, L., Vaitilingom, M., Nicol, E., Baray, J. L., Chaumerliac, N., and Bridoux, M.: Molecular characterization of cloud water samples collected at the Puy de Dome (France) by Fourier transform ion cyclotron resonance mass spectrometry, Environ Sci Technol, 52, 10275-10285, doi:10.1021/acs.est.8b01964, 2018.

Chen, Q., Wang, M., Wang, Y., Zhang, L., Li, Y., and Han, Y.: Oxidative potential of water-soluble matter associated with chromophoric substances in $PM_{2.5}$ over Xi'an, China, Environ Sci Technol, 53, 8574-8584, 10.1021/acs.est.9b01976, 2019.

Cui, M., Li, C., Chen, Y. J., Zhang, F., Li, J., Jiang, B., Mo, Y., Li, J., Yan, C., Zheng, M., Xie, Z., Zhang, G., and Zheng, J.: Molecular characterization of polar organic aerosol constituents in off-road engine emissions using Fourier transform ion cyclotron resonance mass spectrometry (FT-ICR MS): implications for source apportionment, Atmos Chem Phys, 19, 13945-13956, doi:10.5194/acp-19-13945-2019, 2019.

Dasari, S., Andersson, A., Bikkina, S., Holmstrand, H., Budhavant, K., Satheesh, S., Asmi, E., Kesti, J., Backman, J., Salam, A., Bisht, D. S., Tiwari, S., Hameed, Z., and Gustafsson, Ö.: Photochemical degradation affects the light absorption of water-soluble brown carbon in the South Asian outflow, Sci Adv, 5, eaau8066, doi: 10.1126/sciadv.aau8066, 2019.

655 Decesari, S., Facchini, M. C., Matta, E., Mircea, M., Fuzzi, S., Chughtai, A. R., and
656 Smith, D. M.: Water soluble organic compounds formed by oxidation of soot, Atmos
657 Environ, 36, 1827-1832, 10.1016/s1352-2310(02)00141-3, 2002.
658 Di Lorenzo, R. A.; Washenfelder, R. A., Attwood, A. R., Guo, H., Xu, L., Ng, N. L.,
659 Weber, R. J., Baumann, K., Edgerton, E., and Young, C. J.: Molecular-Size-
660 Separated Brown Carbon Absorption for BiomassBurning Aerosol at Multiple Field
661 Sites. Environ Sci Technol, 51, 3128−3137, 10.1021/acs.est.6b06160, 2017.
662 Du, Z., He, K., Cheng, Y., Duan, F., Ma, Y., Liu, J., Zhang, X., Zheng, M., and Weber,
663 R.: A yearlong study of water-soluble organic carbon in Beijing II: Light absorption
664 properties, Atmos Environ, 89, 235-241, 10.1016/j.atmosenv.2014.02.022, 2014.
665 Fan, X. J., Song, J. Z., and Peng, P. A.: Comparison of isolation and quantification
666 methods to measure humic-like substances (HULIS) in atmospheric particles, Atmos.
667 Environ., 60, 366–374, 10.1016/j.atmosenv.2012.06.063, 2012.
668 Fan, X., Song, J., Peng, P.: Comparative study for separation of atmospheric humiclike
669 substance (HULIS) by ENVI-18, HLB, XAD-8 and DEAE sorbents: elemental
670 composition, FT-IR, 1H-NMR and off-line thermochemolysis with
671 tetramethylammonium hydroxide (TMAH). Chemosphere 93, 1710–1719,
672 10.1016/j.chemosphere.2013.05.045, 2013.
673 Fan, X., Song, J., and Peng, P.: Temporal variations of the abundance and optical
674 properties of water soluble Humic-Like Substances (HULIS) in $PM_{2.5}$ at Guangzhou,
675 China, Atmos Res, 172-173, 8-15, doi:10.1016/j.atmosres.2015.12.024, 2016.
676 Fan, X., Cao, T., Yu, X., Wang, Y., Xiao, X., Li, F., Xie, Y., Ji, W., Song, J., and Peng, P:
677 The evolutionary behavior of chromophoric brown carbon during ozone aging of fine

678 particles from biomass burning, Atmos Chem Phys, 20, 4593-4605, doi:10.5194/acp-
679 20-4593-2020, 2020.
680 Graber and Rudich: Atmospheric HULIS: How humic-like are they? A comprehensive
681 and critical review, Atmos Chem Phys, 6, 729-753, 2006.
682 Huang, R. J., Yang, L., Cao, J., Chen, Y., Chen, Q., Chen, Q., Li, Y. J., Duan, J., Zhu, C.
683 C., Dai, W. T., Wang, K., Lin, C. S.;,Ni, H. Y., Corbin, J. C., Wu, Y. F., Zhang, R. J.
684 Tie, X. X., Hoffmann, T., O'Dowd, C., and Dusek, U.: Brown carbon aerosol in
685 urban Xi'an, Northwest China: The composition and light absorption properties,
686 Environ Sci Technol, 52, 6825-6833, doi:10.1021/acs.est.8b02386, 2018.
687 Huang, R. J., Zhang, Y., Bozzetti, C., Ho, K. F., Cao, J. J., Han, Y., Daellenbach, K. R.,
688 Slowik, J. G., Platt, S. M., Canonaco, F., Zotter, P., Wolf, R., Pieber, S. M., Bruns, E.
689 A., Crippa, M., Ciarelli, G., Piazzalunga, A., Schwikowski, M., Abbaszade, G.,
690 Schnelle-Kreis, J., Zimmermann, R., An, Z., Szidat, S., Baltensperger, U., El Haddad,
691 I., and Prevot, A. S.: High secondary aerosol contribution to particulate pollution
692 during haze events in China, Nature, 514, 218-222, 10.1038/nature13774, 2014.
693 Huang, R. J., Yang, L., Shen, J. C., Yuan, W., Gong, Y. Q., Guo, J., Cao, W., Duan, J.,
694 Ni, H., Zhu, C., Dai, W., Li, Y., Chen, Y., Chen, Q., Wu, Y., Zhang, R., Dusek, U.,
695 O'Dowd, C., and Hoffmann, T.: Water-insoluble organics dominate brown carbon in
696 wintertime urban aerosol of China: chemical characteristics and optical properties,
697 Environ Sci Technol, 54, 7836-7847, doi:10.1021/acs.est.0c01149, 2020.
698 Jiang, B., Kuang, B. Y., Liang, Y., Zhang, J., Huang, X. H. H., Xu, C., Yu, J. Z., and Shi,
699 Q.: Molecular composition of urban organic aerosols on clear and hazy days in

Beijing: a comparative study using FT-ICR MS, Environ. Chem., 13, 888–901, https://doi.org/10.1071/en15230, 2016.

Jiang, H., Li, J., Chen, D., Tang, J., Cheng, Z., Mo, Y., Su, T., Tian, C., Jiang, B., Liao, Y., and Zhang, G.: Biomass burning organic aerosols significantly influence the light absorption properties of polarity-dependent organic compounds in the Pearl River Delta Region, China, Environ Int, 144, 106079, 10.1016/j.envint.2020.106079, 2020.

Jiang, H., Li, J., Sun, R., Liu, G., Tian, C., et al. Determining the sources and transport of brown carbon using radionuclide tracers and modeling, J Geophys Res Atmos, 126, e2021JD034616, doi:org/10.1029/2021JD034616, 2021a.

Jiang, H., Li, J., Sun, R., Tian, C., Tang, J., Jiang, B., Liao, Y., Chen, C. E., and Zhang, G.: Molecular dynamics and light absorption properties of atmospheric dissolved organic matter, Environ Sci Technol, 55, 10268–10279, https://doi.org/10.1021/acs.est.1c01770, 2021b.

Kampf, C. J., Filippi, A., Zuth, C., Hoffmann, T., and Opatz, T.: Secondary brown carbon formation via the dicarbonyl imine pathway: nitrogen heterocycle formation and synergistic effects, Phys Chem Chem Phys, 18, 18353-18364, 10.1039/c6cp03029g, 2016.

Kroll, J. H., Donahue, N. M., Jimenez, J. L., Kessler, S. H., Canagaratna, M. R., Wilson, K. R., Altieri, K. E., Mazzoleni, L. R., Wozniak, A. S., Bluhm, H., Mysak, E. R., Smith, J. D., Kolb, C. E., and Worsnop, D. R.: Carbon oxidation state as a metric for describing the chemistry of atmospheric organic aerosol, Nature Chem, 3, 133-139, 10.1038/nchem.948, 2011.

722 Kuang, K. and Shang, J.: Changes in light absorption by brown carbon in soot particles
723 due to heterogeneous ozone aging in a smog chamber, Environ Pollut, 266, 115273,
724 10.1016/j.envpol.2020.115273, 2020.
725 Laskin, A., Laskin, J., and Nizkorodov, S. A.: Chemistry of atmospheric brown carbon,
726 Chem Rev, 115, 4335-4382, 10.1021/cr5006167, 2015.
727 Li, K., Jacob, D. J., Liao, H., Shen, L., Zhang, Q., and Bates, K.H.: Anthropogenic
728 drivers of 2013–2017 trends in summer surface ozone in China, Proc Natl Acad Sci
729 USA, 116, 422–427, https://doi.org/10.1073/pnas.1812168116, 2019.
730 Li, M., Fan, X., Zhu, M., Zou, C., Song, J., Wei, S., Jia, W., and Peng, P.: Abundance
731 and light absorption properties of brown carbon emitted from residential coal
732 combustion in China, Environ Sci Technol, 53, 595-603,
733 doi:10.1021/acs.est.8b05630, 2019.
734 Li, S. W., Chang, M., Li, H., Cui, X. Y., and Ma, L. Q.: Chemical compositions and
735 source apportionment of $PM_{2.5}$ during clear and hazy days: seasonal changes and
736 impacts of Youth Olympic Games, Chemosphere, 256, 127163,
737 10.1016/j.chemosphere.2020.127163, 2020.
738 Lin, P.; Engling, G.; Yu, J. Z.: Humic-like substances in fresh emissions of rice straw
739 burning and in ambient aerosols in the Pearl River Delta Region, China. Atmos
740 Chem Phys, 10, 6487−6500, 10.5194/acp-10-6487-2010, 2010.
741 Lin, P., Bluvshtein, N., Rudich, Y., Nizkorodov, S. A., Laskin, J., and Laskin, A.:
742 Molecular chemistry of atmospheric brown carbon inferred from a nationwide
743 biomass burning event, Environ Sci Technol, 51, 11561-11570,
744 10.1021/acs.est.7b02276, 2017.

745 Lin, P., Rincon, A. G., Kalberer, M., and Yu, J. Z.: Elemental composition of HULIS in
746 the Pearl River Delta Region, China: results inferred from positive and negative
747 electrospray high resolution mass spectrometric data, Environ Sci Technol, 46, 7454-
748 7462, 10.1021/es300285d, 2012.
749 Lin, P., Fleming, L. T., Nizkorodov, S. A., Laskin, J., and Laskin，A.: Comprehensive
750 molecular characterization of atmospheric brown carbon by high resolution mass
751 spectrometry with electrospray and atmospheric pressure photoionization, Anal
752 Chem, 90, 12493-12502. doi:10.1021/acs.analchem.8b02177, 2018.
753 Liu, J., Lin, P., Laskin, A., Laskin, J., Kathmann, S. M., Wise, M., Caylor, R., Imholt, F.,
754 Selimovic, V., and Shilling, J. E.: Optical properties and aging of light-absorbing
755 secondary organic aerosol, Atmos Chem Phys, 16, 12815-12827, 10.5194/acp-16-
756 12815-2016, 2016.
757 Liu, J., Mo, Y., Ding, P., Li, J., Shen, C., and Zhang, G.: Dual carbon isotopes ((14)C
758 and (13)C) and optical properties of WSOC and HULIS-C during winter in
759 Guangzhou, China, Sci Total Environ, 633, 1571-1578,
760 10.1016/j.scitotenv.2018.03.293, 2018.
761 Ma, Y., Cheng, Y., Qiu, X., Cao, G., Kuang, B., Yu, J. Z., and Hu, D.: Optical properties,
762 source apportionment and redox activity of humic-like substances (HULIS) in
763 airborne fine particulates in Hong Kong, Environ Pollut, 255, 113087,
764 10.1016/j.envpol.2019.113087, 2019.
765 Mo, Y., Li, J., Jiang, B., Su, T., Geng, X., Liu, J., Jiang, H., Shen, C., Ding, P., Zhong, G.,
766 Cheng, Z., Liao, Y., Tian, C., Chen, Y., and Zhang, G.: Sources, compositions, and
767 optical properties of humic-like substances in Beijing during the 2014 APEC summit:

768 Results from dual carbon isotope and Fourier-transform ion cyclotron resonance
769 mass spectrometry analyses, Environ Pollut, 239, 322-331,
770 10.1016/j.envpol.2018.04.041, 2018.
771 Mohr, C., Lopez-Hilfiker, F. D., Zotter, P., Prevot, A. S., Xu, L., Ng, N. L., Herndon, S.
772 C., Williams, L. R., Franklin, J. P., Zahniser, M. S., Worsnop, D. R., Knighton, W.
773 B., Aiken, A. C., Gorkowski, K. J., Dubey, M. K., Allan, J. D., and Thornton, J. A.:
774 Contribution of nitrated phenols to wood burning brown carbon light absorption in
775 Detling, United Kingdom during winter time, Environ Sci Technol, 47, 6316-6324,
776 10.1021/es400683v, 2013.
777 Ni, H., Huang, R. J., Pieber, S. M., Corbin, J. C., Stefenelli, G., Pospisilova, V., Klein, F.,
778 Gysel-Beer, M., Yang, L., Baltensperger, U., Haddad, I. E., Slowik, J. G., Cao, J.,
779 Prevot, A. S. H., and Dusek, U.: Brown carbon in primary and aged coa lcombustion
780 emission, Environ Sci Technol, 55, 5701-5710, 10.1021/acs.est.0c08084, 2021.
781 Qin, J., Zhang, L., Qin, Y., Shi, S., Li, J., Gao, Y., Tan, J., and Wang, X.: pH-Dependent
782 Chemical Transformations of Humic-Like Substances and Further Cognitions
783 Revealed by Optical Methods. Environ Sci Technol, 56, 7578-7587,
784 10.1021/acs.est.1c07729, 2022.
785 Shen, Z., Zhang, Q., Cao, J., Zhang, L., Lei, Y., Huang, Y., Huang, R. J., Gao, J., Zhao,
786 Z., Zhu, C., Yin, X., Zheng, C., Xu, H., and Liu, S.: Optical properties and possible
787 sources of brown carbon in PM 2.5 over Xi'an, China, Atmos Environ, 150, 322-330,
788 10.1016/j.atmosenv.2016.11.024, 2017.
789 Song, J.: Data for SJ, Harvard Dataverse [data set],
790 (https://doi.org/10.7910/DVN/DYGYQT, 2022.

Song, J. Z., Li, M. J., Fan, X. J., Zou, C. L., Zhu, M. B., Jiang, B., Yu, Z. Q., Jia, W. L., Liao, Y. H., and Peng, P. A.: Molecular characterization of water- and methanol-soluble organic compounds emitted from residential coal combustion using ultrahigh-resolution electrospray ionization Fourier transform ion cyclotron resonance mass spectrometry, Environ Sci Technol, 53, 13607-13617, 10.1021/acs.est.9b04331, 2019.

Song, J. Z., Li, M. J., Jiang, B., Wei, S. Y., Fan, X. J., and Peng, P. A.: Molecular Characterization of Water-Soluble Humic like substances in smoke particles emitted from combustion of biomass materials and coal using ultrahigh-resolution electrospray ionization Fourier transform ion cyclotron resonance mass spectrometry, Environ Sci Technol, 52, 2575-2585, 10.1021/acs.est.7b06126, 2018.

Song, J. Z., Li, M. J., Zou, C. L., Cao, T., Fan, X. J., Jiang, B., Yu, Z. Q., Jia, W. L., and Peng, P. A.: Molecular characterization of nitrogen-containing compounds in humic-like substances emitted from biomass burning and coal combustion, Environ Sci Technol, 56, 119-130, doi:10.1021/acs.est.1c04451, 2022.

Sumlin, B. J., Pandey, A., Walker, M. J., Pattison, R. S., Williams, B. J., and Chakrabarty, R. K.: Atmospheric photooxidation diminishes light absorption by primary brown carbon aerosol from biomass burning, Environ Sci Tech Let, 4, 540-545, 10.1021/acs.estlett.7b00393, 2017.

Surratt, J. D., Gomez-Gonzalez, Y., Chan, A. W. H., Vermeylen, R., Shahgholi, M., Kleindienst, T. E., Edney, E. O., Offenberg, J. H., Lewandowski, M., Jaoui, M., Maenhaut, W., Claeys, M., Flagan, R. C., and Seinfeld, J. H.: Organosulfate

formation in biogenic secondary organic aerosol, J Phys Chem A, 112, 8345-8378, 10.1021/jp802310p, 2008.

Tan, J., Xiang, P., Zhou, X., Duan, J., Ma, Y., He, K., Cheng, Y., Yu, J., and Querol, X.: Chemical characterization of humic-like substances (HULIS) in $PM_{2.5}$ in Lanzhou, China, Sci Total Environ, 573, 1481-1490, 10.1016/j.scitotenv.2016.08.025, 2016.

Tang, J., Li, J., Su, T., Han, Y., Mo, Y. Z., Jiang, H. X., Cui, M., Jiang, B., Chen, Y. J., Tang, J. H., Song, J. Z., Peng, P. A., and Zhang, G.: Molecular compositions and optical properties of dissolved brown carbon in biomass burning, coal combustion, and vehicle emission aerosols illuminated by excitation-emission matrix spectroscopy and Fourier transform ion cyclotron resonance mass spectrometry analysis, Atmos Chem Phys, 20, 2513-2532, 10.5194/acp-20-2513-2020, 2020.

Tomaz, S., Cui, T., Chen, Y., Sexton, K. G., Roberts, J. M., Warneke, C., Yokelson, R. J., Surratt, J. D., and Turpin, B. J.: Photochemical Cloud Processing of primary wildfire emissions as a ptential source of secondary organic Aerosol, Environ Sci Technol, 52, 11027-11037, 10.1021/acs.est.8b03293, 2018.

Tong, H., Zhang, Y., Filippi, A., Wang, T., Li, C., Liu, F., Leppla, D., Kourtchev, I., Wang, K., Keskinen, H. M., Levula, J. T., Arangio, A. M., Shen, F., Ditas, F., Martin, S. T., Artaxo, P., Godoi, R. H. M., Yamamoto, C. I., de Souza, R. A. F., Huang, R. J., Berkemeier, T., Wang, Y., Su, H., Cheng, Y., Pope, F. D., Fu, P., Yao, M., Pohlker, C., Petaja, T., Kulmala, M., Andreae, M. O., Shiraiwa, M., Poschl, U., Hoffmann, T., and Kalberer, M.: Radical formation by fine particulate matter associated with highly oxygenated molecules, Environ Sci Technol, 53, 12506-12518, 10.1021/acs.est.9b05149, 2019.

836 Wang, J., Wang, G., Gao, J., Wang, H., Ren, Y., Li, J., Zhou, B., Wu, C., Zhang, L.,
837 Wang, S., and Chai, F.: Concentrations and stable carbon isotope compositions of
838 oxalic acid and related SOA in Beijing before, during, and after the 2014 APEC,
839 Atmos Chem Phys, 17, 981-992, 10.5194/acp-17-981-2017, 2017a.
840 Wang, X. K., Hayeck, N., Bruggemann, M., Yao, L., Chen, H. F., Zhang, C., Emmelin,
841 C., Chen, J. M., George, C., and Wang, L.: Chemical characteristics of organic
842 aerosols in shanghai: a study by ultrahigh-performance liquid chromatography
843 coupled with orbitrap mass spectrometry, J Geophy Res Atmos, 122, 11703-11722,
844 10.1002/2017jd026930, 2017b.
845 Wang, Y., Hu, M., Lin, P., Tan, T., Li, M., Xu, N., Zheng, J., Du, Z., Qin, Y., Wu, Y., Lu,
846 S., Song, Y., Wu, Z., Guo, S., Zeng, L., Huang, X., and He, L.: Enhancement in
847 particulate organic nitrogen and light absorption of humic-like substances over
848 Tibetan Plateau due to long-range transported biomass burning emissions, Environ
849 Sci Technol, 53, 14222-14232, 10.1021/acs.est.9b06152, 2019.
850 Wang, X., Hayeck, N., Brüggemann, M., Abis, L., Riva, M., Lu, Y., Wang, B., Chen, J.,
851 George, C., and Wang, L.: Chemical characteristics and brown carbon chromophores
852 of atmospheric organic aerosols over the Yangtze River channel: a cruise campaign,
853 J Geophy Res Atmos, 125, 10.1029/2020jd032497, 2020.
854 Win, M. S., Zeng, J., Yao, C., Zhao, M., Xiu, G., Xie, T., Rao, L., Zhang, L., Lu, H., Liu,
855 X., Wang, Q., and Lu, S.: Sources of HULIS-C and its relationships with trace
856 metals, ionic species in PM2.5 in suburban Shanghai during haze and non-haze days,
857 Journal of Atmospheric Chemistry, 77, 63-81, 10.1007/s10874-020-09404-7, 2020.

Wong, J. P. S., Nenes, A., and Weber, R. J.: Changes in Light Absorptivity of Molecular Weight Separated Brown Carbon Due to Photolytic Aging, Environ Sci Technol, 51, 8414-8421, 10.1021/acs.est.7b01739, 2017.

Wong, J. P. S., Tsagkaraki, M., Tsiodra, I., Mihalopoulos, N., Violaki, K., Kanakidou, M., Sciare, J., Nenes, A., and Weber, R. J.: Effects of atmospheric processing on the oxidative potential of biomass burning organic aerosols, Environ Sci Technol, 53, 6747-6756, 10.1021/acs.est.9b01034, 2019.

Wu, Z., Wang, Y., Tan, T., Zhu, Y., Li, M., Shang, D., Wang, H., Lu, K., Guo, S., Zeng, L., and Zhang, Y.: Aerosol liquid water driven by anthropogenic inorganic salts: implying its key role in haze formation over the North China Plain, Environ Sci Technol Lett, 5, 160-166, 10.1021/acs.estlett.8b00021, 2018.

Yang, X., Lu, K., Ma, X., Gao, Y., Tan, Z., Wang, H., Chen, X., Li, X., Huang, X., He, L., Tang, M., Zhu, B., Chen, S., Dong, H., Zeng, L., and Zhang, Y.: Radical chemistry in the Pearl River Delta: observations and modeling of OH and HO_2 radicals in Shenzhen in 2018. Atmos Chem Phys, 22, 12525-12542, 10.5194/acp-22-12525-2022, 2022.

Yu, L., Smith, J., Laskin, A., George, K. M., Anastasio, C., Laskin, J., Dillner, A. M., and Zhang, Q.: Molecular transformations of phenolic SOA during photochemical aging in the aqueous phase: competition among oligomerization, functionalization, and fragmentation, Atmos Chem Phys, 16, 4511-4527, 10.5194/acp-16-4511-2016, 2016.

Yu, X., Yu, Q., Zhu, M., Tang, M., Li, S., Yang, W., Zhang, Y., Deng, W., Li, G., Yu, Y., Huang, Z., Song, W., Ding, X., Hu, Q., Li, J., Bi, X., and Wang, X.: Water soluble

organic nitrogen (WSON) in ambient fine particles over a megacity in South China: spatiotemporal variations and source apportionment, J Geophy Res Atmos, 122, 10.1002/2017jd027327, 2017.

Yuan, W., Huang, R. J., Yang, L., Ni, H., Wang, T., Cao, W., Duan, J., Guo, J., Huang, H., and Hoffmann, T.: Concentrations, optical properties and sources of humic-like substances (HULIS) in fine particulate matter in Xi'an, Northwest China, Sci Total Environ, 789, 147902, 10.1016/j.scitotenv.2021.147902, 2021.

Zeng, Y., Shen, Z., Takahama, S., Zhang, L., Zhang, T., Lei, Y., Zhang, Q., Xu, H., Ning, Y., Huang, Y., Cao, J., and Rudolf, H.: Molecular Absorption and Evolution Mechanisms of PM 2.5 Brown carbon revealed by electrospray ionization Fourier transform–ion cyclotron resonance mass spectrometry during a severe winter pollution episode in Xi'an, China, Geophy Res Lett, 47, 10.1029/2020gl087977, 2020.

Zeng, Y. L., Ning, Y. L., Shen, Z. X., Zhang, L. M., Zhang, T., Lei, Y. L., Zhang, Q., Li, G. H., Xu, H. M., Ho, S. S. H., and Cao, J. J.: The roles of N, S, and O in molecular absorption features of brown carbon in $PM_{2.5}$ in a typical semi-arid megacity in Northwestern China, J Geophys Res Atmos, 126, 2021.

Zhang, J., Liu, L., Xu, L., Lin, Q., Zhao, H., Wang, Z., Guo, S., Hu, M., Liu, D., Shi, Z., Huang, D., and Li, W.: Exploring wintertime regional haze in northeast China: role of coal and biomass burning, Atmos Chem Phys, 20, 5355-5372, 10.5194/acp-20-5355-2020, 2020.

Zhang, L., Wang, G., Wang, J., Wu, C., Cao, C., and Li, J.: Chemical composition of fine particulate matter and optical properties of brown carbon before and during

heating season in Xi'an, Journal of Earth Environment, 8, 451-458, 2017.

Zhang, Q., Worsnop, D. R., Canagaratna, M. R., and Jimenez, J. L.: Hydrocarbon-like and oxygenated organic aerosols in Pittsburgh: insights into sources and processes of organic aerosols, Atmos Chem Phys, 5, 3289-3311, 10.5194/acp-5-3289-2005, 2005.

Zhang, Y.-L., El-Haddad, I., Huang, R.-J., Ho, K.-F., Cao, J.-J., Han, Y., Zotter, P., Bozzetti, C., Daellenbach, K. R., Slowik, J. G., Salazar, G., Prévôt, A. S. H., and Szidat, S.: Large contribution of fossil fuel derived secondary organic carbon to water soluble organic aerosols in winter haze in China, Atmos Chem Phys, 18, 4005-4017, 10.5194/acp-18-4005-2018, 2018.

Zhong, M. and Jang, M.: Dynamic light absorption of biomass-burning organic carbon photochemically aged under natural sunlight, Atmos Chem Phys, 14, 1517-1525, 10.5194/acp-14-1517-2014, 2014.

Zhu, C. S., Cao, J. J., Huang, R. J., Shen, Z. X., Wang, Q. Y., and Zhang, N. N.: Light absorption properties of brown carbon over the southeastern Tibetan Plateau, Sci Total Environ, 625, 246-251, 10.1016/j.scitotenv.2017.12.183, 2018.

Zou, C., Li, M., Cao, T., Zhu, M., Fan, X., Peng, S., Song, J., Jiang, B., Jia, W., Yu, C., Song, H., Yu, Z., Li, J., Zhang, G., and Peng, P. a.: Comparison of solid phase extraction methods for the measurement of humic-like substances (HULIS) in atmospheric particles, Atmos Environ, 225, 117370, 10.1016/j.atmosenv.2020.117370, 2020.

Table 1. Formular number of potential BrC chromophores and the intensity ratios of each group of potential BrC in total potential BrC and each group of total identified formulas, respectively.

Samples	Elemental compositions	Number	ESI- Int_C/Int_{BrC}	ESI- $Int_{BrC,i}/Int_{bulk}$	Elemental compositions	Number	ESI+ Int_C/Int_{BrC}	ESI+ $Int_{BrC,i}/Int_{bulk}$
Clean-I	CHO-	424	**0.48**	**0.25**	CHO+	263	**0.37**	0.07
	CHON-	773	**0.46**	**0.53**	CHON+	480	**0.56**	**0.15**
	CHOS-	63	0.03	0.05	CHN+	79	0.07	**0.56**
	CHONS-	43	0.03	0.08	all in ESI+	822		**0.11**
	all in ESI-	1303		**0.26**				
Haze-I	CHO-	356	**0.44**	**0.21**	CHO+	244	**0.29**	0.09
	CHON-	791	**0.50**	**0.45**	CHON+	614	**0.62**	**0.22**
	CHOS-	43	0.03	0.03	CHN+	94	0.09	**0.39**
	CHONS-	39	0.03	0.07	all in ESI+	952		**0.16**
	all in ESI-	1229		**0.22**				
Haze-II	CHO-	444	**0.45**	**0.26**	CHO+	333	**0.34**	0.06
	CHON-	941	**0.49**	**0.49**	CHON+	595	**0.56**	**0.13**
	CHOS-	67	0.03	0.03	CHN+	89	0.1	**0.48**
	CHONS-	78	0.03	0.07	all in ESI+	1017		**0.10**
	all in ESI-	1530		**0.25**				
Clean-II	CHO-	391	**0.46**	**0.27**	CHO+	234	**0.38**	0.09
	CHON-	707	**0.48**	**0.59**	CHON+	462	**0.56**	**0.18**
	CHOS-	64	0.03	0.05	CHN+	75	0.06	**0.57**
	CHONS-	49	0.03	0.10	all in ESI+	771		**0.13**
	all in ESI-	1211		**0.29**				

Int_C: the intensity of each group of identified potential BrC;
Int_{BrC}: the sum intensity of identified potential BrC;
Int_{Bulk}: the sum intensity of each group of total identified formulas.

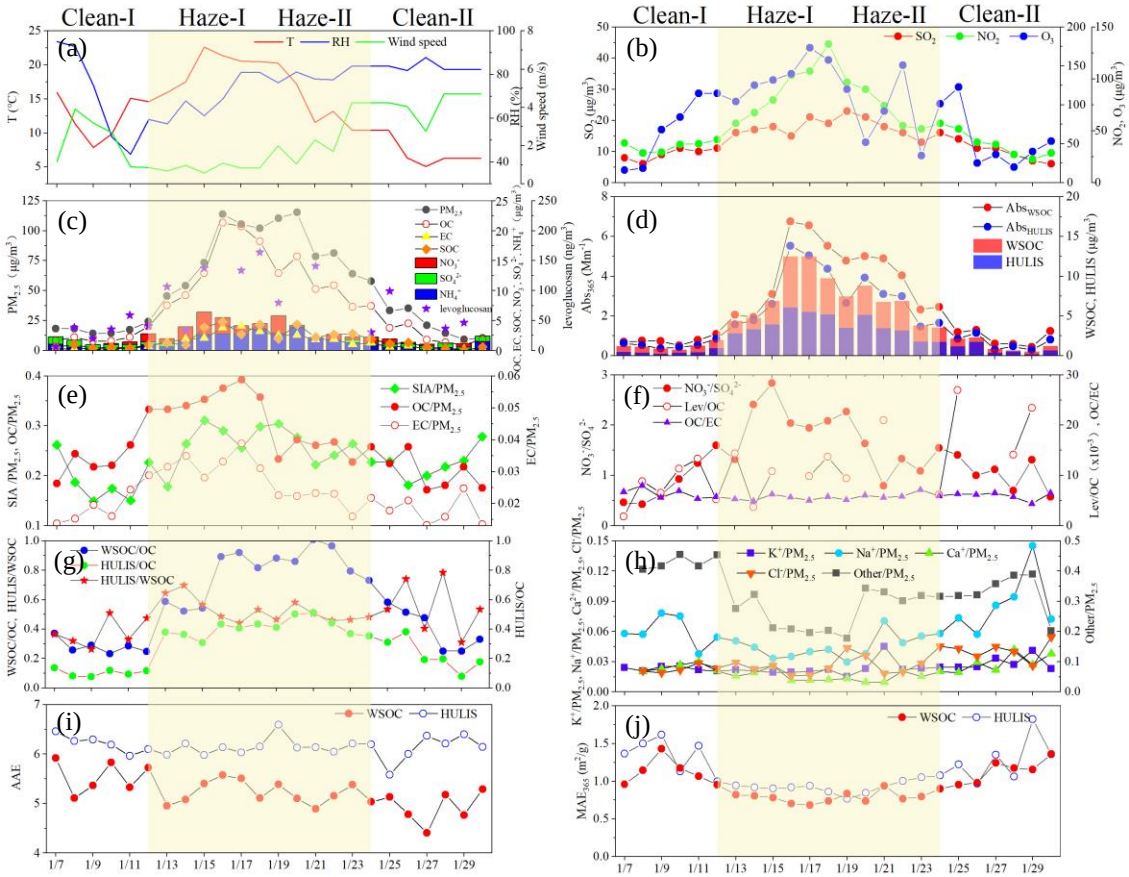

Figure 1. Temporal variation in meteorological parameters, concentrations of chemical composition, and optical properties (Abs_{365}, MAE_{365}, and AAE) of water-soluble BrC in the $PM_{2.5}$ samples.

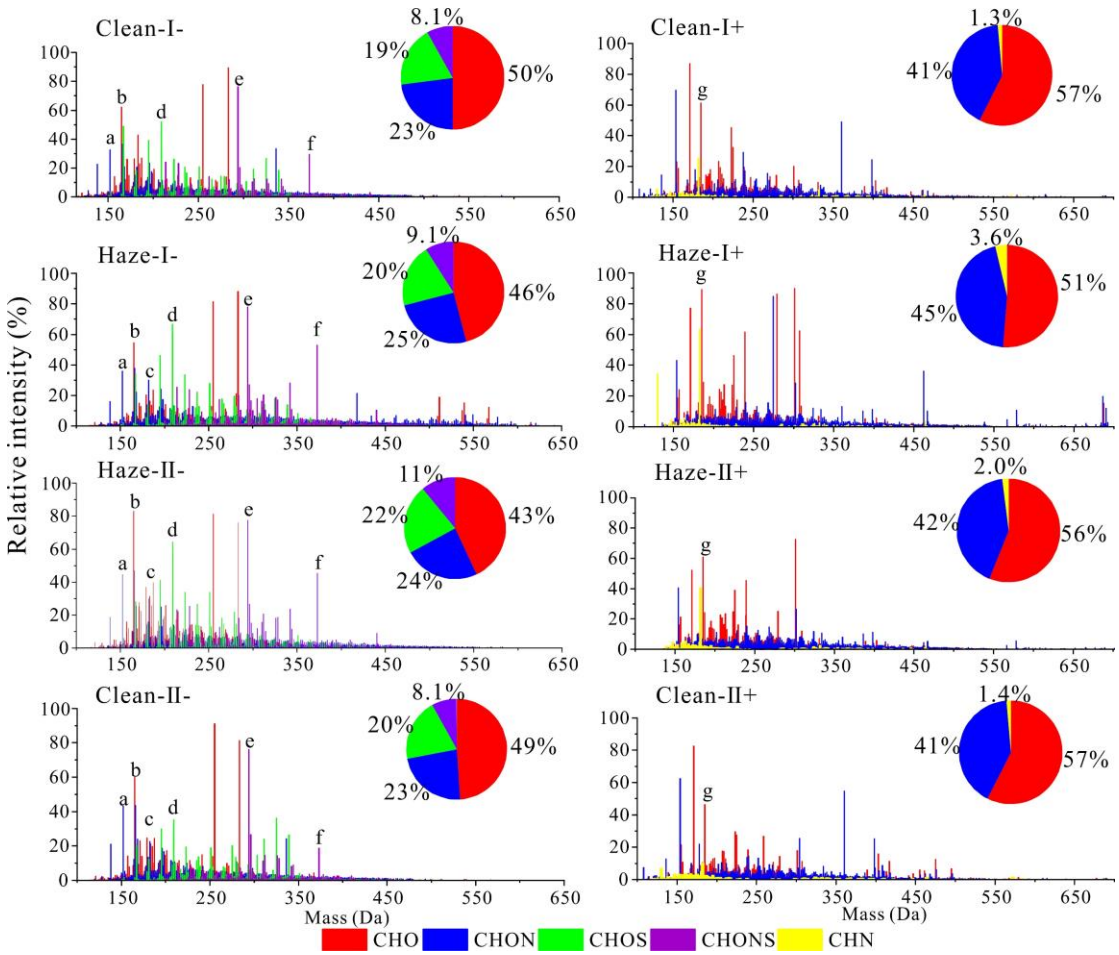

Figure 2. Mass spectra of HULIS detected in ESI- and ESI+ modes during the haze process. The pie charts represent the intensity percent of different compound groups.

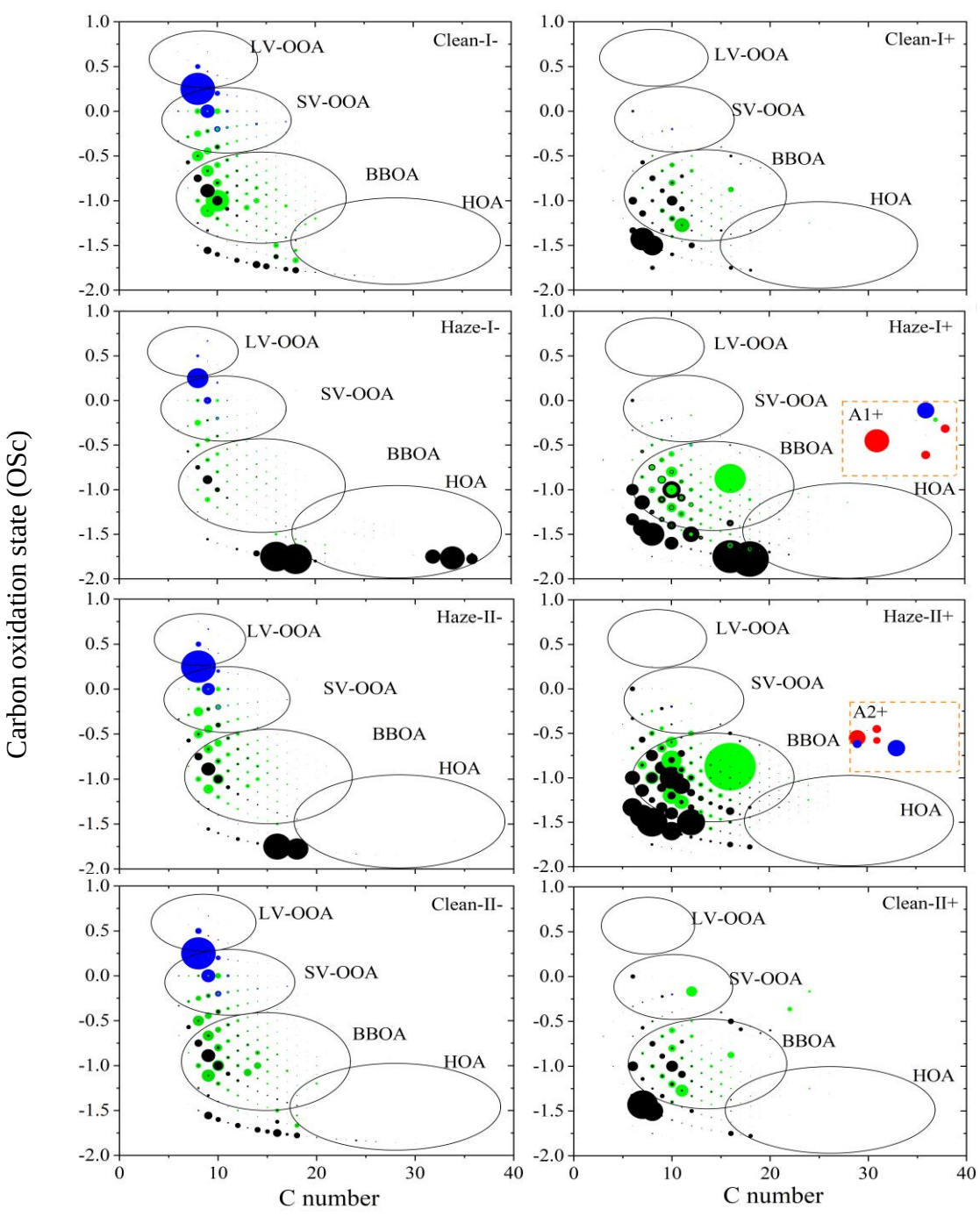

Figure 3. Carbon oxidation state (OSc) plots for CHO- and CHO+. Formulas with black, green, blue, and red are assigned to aliphatic (AI = 0), olefinic (0< AI <0.5), aromatic (0.5≤ AI <0.67), and condensed aromatic (AI ≥0.67) species (Koch and Dittmar, 2006), respectively.

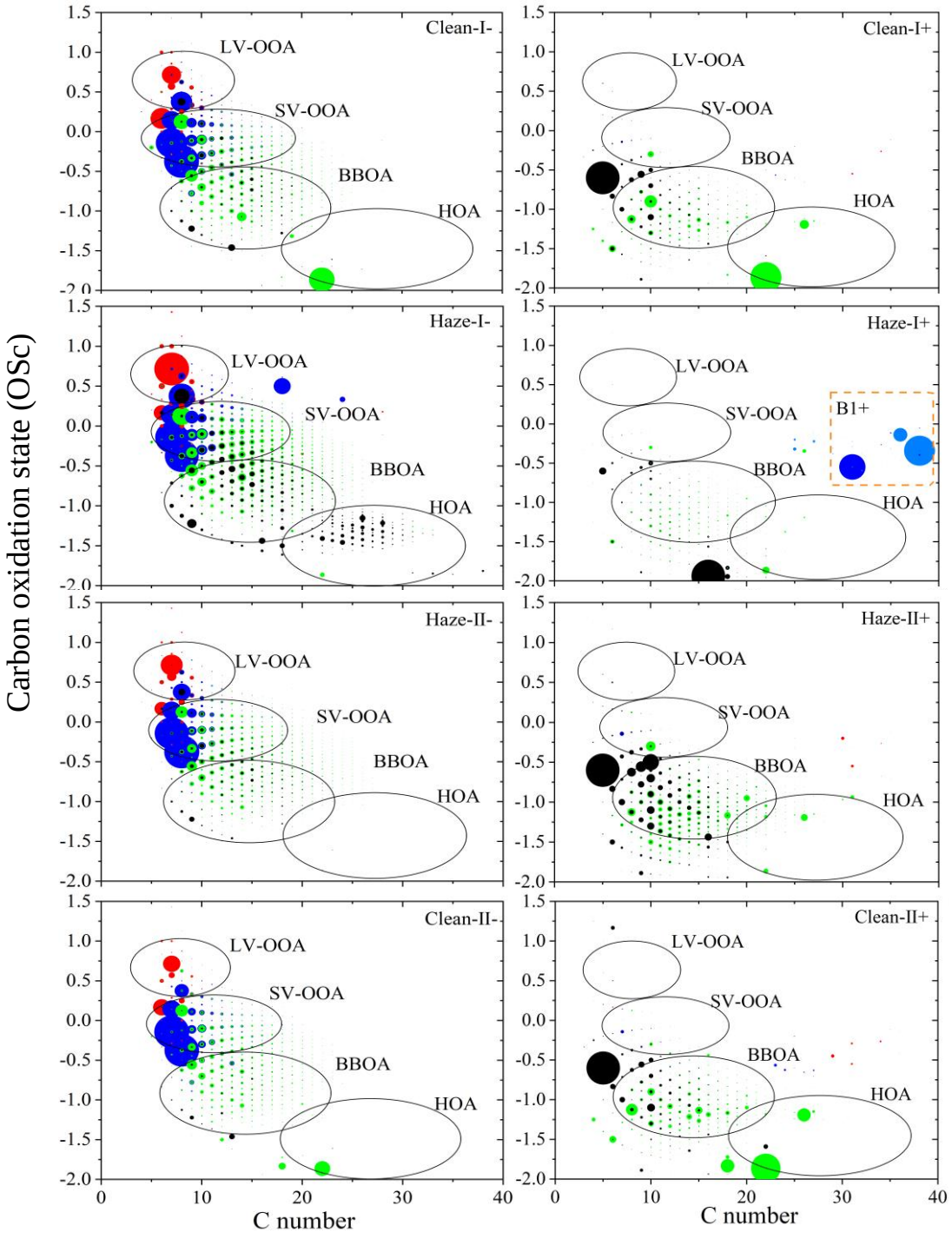

Figure 4. Carbon oxidation state (OSc) plots for CHON- and CHON+. Formulas with black, green, blue, and red are assigned to aliphatic (AI = 0), olefinic (0< AI <0.5), aromatic (0.5≤ AI <0.67), and condensed aromatic (AI ≥0.67) species (Koch and Dittmar, 2006), respective.

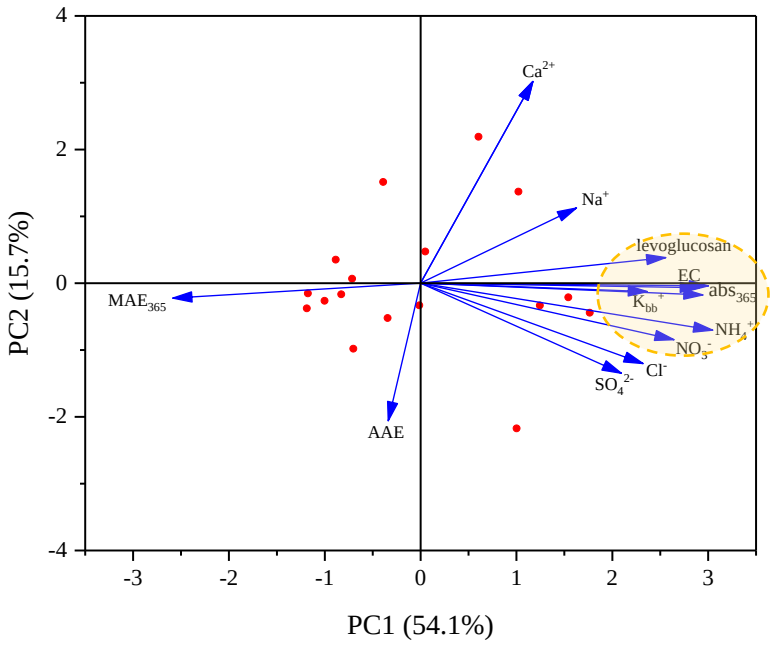

Figure 5. Principal component analysis results for the optical properties of HULIS and chemical compositions of $PM_{2.5}$.